Available online at www.sciencedirect.com
SCIENCE DIRECT®
Icarus 170 (2004) 424–429
ICARUS
www.elsevier.com/locate/icarus

Hydrogen peroxide on Mars: evidence for spatial and seasonal variations

Th. Encrenaz [a,*,1], B. Bézard [a], T.K. Greathouse [b], M.J. Richter [c], J.H. Lacy [b], S.K. Atreya [d], A.S. Wong [d], S. Lebonnois [e], F. Lefèvre [f], F. Forget [e]

[a] *LESIA, Observatoire de Paris, F-92195 Meudon, France*
[b] *Department of Astronomy, University of Texas at Austin, RLM 15.308, C-1400 Austin, TX 78712-1083, USA*
[c] *Physics Department, University of California, One Shields Ave., Davis, CA 95616, USA*
[d] *Department of Atmospheric, Oceanic, and Space Sciences, University of Michigan, Ann Arbor, MI 48109-2143, USA*
[e] *IPSL/Laboratoire de Météorologie Dynamique, place Jussieu, F-75231 Paris cedex 05, France*
[f] *IPSL/Service d'Aéronomie, place Jussieu, F-75231 Paris cedex 05, France*

Received 4 March 2004; revised 28 April 2004

Available online 17 June 2004

Abstract

Hydrogen peroxide (H_2O_2) has been suggested as a possible oxidizer of the martian surface. Photochemical models predict a mean column density in the range of 10^{15}–10^{16} cm^{-2}. However, a stringent upper limit of the H_2O_2 abundance on Mars (9×10^{14} cm^{-2}) was derived in February 2001 from ground-based infrared spectroscopy, at a time corresponding to a maximum water vapor abundance in the northern summer (30 pr. μm, $Ls = 112°$). Here we report the detection of H_2O_2 on Mars in June 2003, and its mapping over the martian disk using the same technique, during the southern spring ($Ls = 206°$) when the global water vapor abundance was ∼ 10 pr. μm. The spatial distribution of H_2O_2 shows a maximum in the morning around the sub-solar latitude. The mean H_2O_2 column density (6×10^{15} cm^{-2}) is significantly greater than our previous upper limit, pointing to seasonal variations. Our new result is globally consistent with the predictions of photochemical models, and also with submillimeter ground-based measurements obtained in September 2003 ($Ls = 254°$), averaged over the martian disk (Clancy et al., 2004, Icarus 168, 116–121).

Keywords: Mars; Mars, atmosphere; Atmospheres, composition; Infrared observations; Photochemistry

1. Introduction

H_2O_2 has been proposed as an oxidizer of the martian regolith, which may have sterilized the soil down to a few meters below the surface (Bullock et al., 1994). It could have been responsible for the absence of organic molecules on the surface of Mars (Oyama et al., 1977), and possibly also for the positive response of the Viking Labeled Release Life Science Experiment (Huguenin, 1982; Levin and Straat, 1988). In fact, photochemical models have predicted the formation of H_2O_2 in the atmosphere of Mars with a typical global average column abundance in the range of 10^{15}–10^{16} cm^{-2} (Krasnopolsky, 1993, 1995; Atreya and Gu, 1994; Nair et al., 1994; Clancy and Nair, 1996). In these models, H_2O_2 results from the combination of two HO_2 radicals which result from a reaction involving H, O_2, and CO_2:

$$H + O_2 + CO_2 \rightarrow HO_2 + CO_2,$$

$$HO_2 + HO_2 \rightarrow H_2O_2 + O_2.$$

The destruction of H_2O_2 occurs through its photodissociation into OH:

$$H_2O_2 + h\nu \rightarrow 2OH.$$

Since H is produced from the photolysis of water vapor, to first order, photochemical models expect H_2O and H_2O_2 abundances to be correlated, if all else were equal. Any correlation between H_2O_2 and H_2O will be at a given altitude, not necessarily in the column integrated sense. It should be mentioned that our observations allow to measurement of

* Corresponding author. Fax: 33-1-45-07-28-06.
E-mail address: therese.encrenaz@obspm.fr (Th. Encrenaz).

[1] Visiting Astronomer at the Infrared Telescope Facility, which is operated by the University of Hawaii under Cooperative Agreement NCC 5-538 with the National Aeronautics and Space Administration, Office of Space Science, Planetary Astronomy Program.

0019-1035/$ – see front matter
doi:10.1016/j.icarus.2004.05.008

the column abundance of H_2O_2. We will elaborate on this point and on the seasonal variability of H_2O_2 further in Section 4.

Previous attempts to detect H_2O_2 on Mars were unsuccessful, until its very recent detection from submillimeter ground-based spectroscopy (Clancy et al., 2004). A 2-σ upper limit of 7.5×10^{15} cm^{-2} for H_2O_2 was obtained first by Krasnopolsky et al. (1997), corresponding to a mean H_2O abundance of ~ 10 pr. μm and $Ls = 222°$. A more stringent 2-σ upper limit of 9×10^{14} cm^{-2} was obtained by Encrenaz et al. (2002), corresponding to a mean H_2O abundance of ~ 30 pr. μm and $Ls = 112°$. In both cases, the estimated column density of water vapor was inferred from the global measurements obtained by the MAWD Viking experiment (Jakosky and Haberle, 1992), later confirmed by the TES instrument aboard Mars Global Surveyor and well reproduced by climatological models (Forget et al., 1999). Both observations were done using ground-based high-resolution infrared spectroscopy at a wavelength of ~ 8 μm in the ν_6 fundamental vibration-rotation band of H_2O_2. In the case of Mars, molecular lines are very narrow with a FWHM typically less than 0.001 cm^{-1}, so that high spectral resolving power ($R > 10^4$) is essential. This constraint prevents infrared or submillimeter detection of H_2O_2 from spacecraft, which do not carry such facility. The 8-μm spectral range is best suited to search for H_2O_2 on Mars using ground-based telescopes, due to the relatively large intensity of individual H_2O_2 transitions in the ν_6 band, coupled with the availability of high-resolution spectrometers.

In this paper, we present the detection and mapping of H_2O_2 on Mars in June 2003 (Encrenaz et al., 2003), using the same technique as in our previous attempt (Encrenaz et al., 2002). Several individual H_2O_2 lines have been identified, and the resulting H_2O_2 column density in the region close to the sub-solar point is found to be $\sim 7.5 \times 10^{15}$ cm^{-2}. Using the ground-based submillimeter heterodyne technique, Clancy et al. (2004) first reported the detection of H_2O_2 obtained ten weeks later, in September 2003.

2. Observations

Observations of Mars were carried out on June 19–20, 2003 using the Texas Echelon Cross Echelle Spectrograph (TEXES) mounted at the 3-m NASA/Infrared Telescope Facility (IRTF). TEXES is a mid-infrared spectrograph covering the 5- to 25-μm range and it has high spectral and spatial resolution capabilities (Lacy et al., 2002). We used the high-resolution cross-dispersed mode. On June 19, we covered the 1230–1236 cm^{-1} (8.09–8.13 μm) spectral range and on June 20, the 1237–1244 cm^{-1} (8.04–8.08 μm) spectral range. In both cases, we used a 1.1×8 arcsec slit; the spectral resolution was 0.016 cm^{-1}, corresponding to a resolving power of 7.7×10^4.

The diameter of Mars was 15 arcsec at the time of our observations. The aerocentric longitude Ls was 206° (beginning of southern spring). The latitudes of the sub-solar point and the sub-Earth point were −11° and −21°, respectively. The total observing time (summed over the two nights) was 260 minutes, over which the sub-solar point spanned the longitude range of 97° W–155° W. Mars was approaching the Earth with a radial velocity of −11 km s^{-1}, corresponding to a Doppler shift of +0.045 cm^{-1}. According to Viking (Jakosky and Haberle, 1992) and MGS (Smith, 2002) global measurements, the global water vapor abundance was ~ 10 pr. μm.

For both data sets, the slit was oriented along the celestial N–S axis, and the telescope was stepped by 0.5″ E between two successive 8-sec integrations. The slit covered alternatively the northern and the southern parts of the martian disk, in order to build two maps, for the northern and southern hemispheres, respectively. The pixel size was 0.33 arcsec; our spatial resolution, after binning, is about 1.5 arcsec.

The flux calibration of the TEXES spectra follows the radiometric method used commonly for millimeter and submillimeter observations (Rohlfs and Wilson, 2004), and is described in Encrenaz et al. (2002). The data are uncorrected for telluric absorption in order to preserve the original S/N ratio. Spectra of the Moon were recorded for identifying telluric absorptions.

Figure 1 shows spectra of Mars in the 1230.0–1236.0 cm^{-1} range (Fig. 1a) and the 1237.2–1243.5 cm^{-1} range (Fig. 1b). To obtain these spectra, we averaged individual spectra over an area of Mars where the H_2O_2 line depths (in radiance units) were found to be maximum, in order to maximize the accuracy of the H_2O_2 measurement. This area covers the latitude range 10° N–35° S, and the longitude range 20° E–30° W relative to the sub-solar point. The averaged spectra, incorporate 1023 (Fig. 1a) and 1657 (Fig. 1b) individual spectra, respectively. We note that the continuum flux in the selected area (55–59 erg s^{-1} cm^{-2} sr^{-1}/cm^{-1}) corresponds to a brightness temperature of 300 K, slightly higher than that expected from the Laboratoire de Météorologie Dynamique and Oxford University martian Global Climate Model (hereafter GCM; Forget et al., 1999), which is ~ 290 K. We attribute this difference to the uncertainty in the absolute calibration of our data.

Several individual H_2O_2 lines are identified in both spectral intervals. In particular, a doublet can be clearly seen at 1234.05 and 1234.10 cm^{-1} (Doppler-shifted positions, Fig. 2). This doublet was not detected in our previous observations of February 2001 (see Figs. 3–4 of Encrenaz et al., 2002). We note, however, that the line at 1234.05 cm^{-1} is shifted by one resolution element, or ~ 0.015 cm^{-1}, relative to the predicted H_2O_2 line position. At this time, we have no satisfactory explanation for this offset. The two strongest H_2O_2 transitions of the entire spectral range appear prominently at 1241.57 and 1241.65 cm^{-1} as seen in Fig. 3. All other lines in Fig. 1 are identified as martian CO_2 lines belonging to weak $^{12}C^{16}O^{18}O$ and $^{13}C^{16}O^{18}O$ isotopic bands, or as telluric absorption lines.

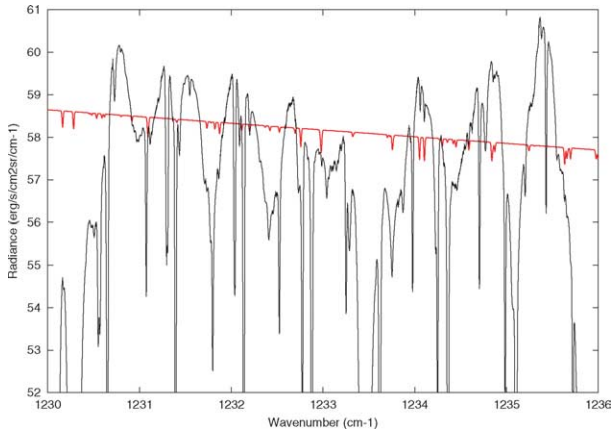

Fig. 1. Spectra of Mars (black line) integrated over a selected area around the sub-solar point, and uncorrected for telluric absorptions. The spectral resolution is 0.016 cm^{-1}. (a) 1230.0–1236.0 cm^{-1} range; (b) 1237.2–1243.5 cm^{-1} ranges. The synthetic absorption spectrum of H_2O_2, corresponding to a mixing ratio of 4×10^{-8}, is shown for comparison (red line). All the lines in both spectra can be interpreted as CO_2 or H_2O_2 martian lines, or as terrestrial lines. The strongest absorption lines are due to telluric methane lines.

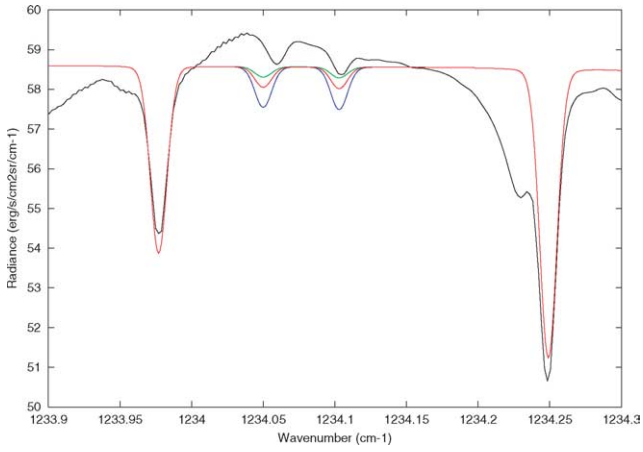

Fig. 2. Spectrum at 1233.9–1234.3 cm^{-1} in the selected area of the martian disk (black line). The Doppler shift is 0.045 cm^{-1}. Models correspond to H_2O_2 mean vertical mixing ratios of 2×10^{-8} (green), 4×10^{-8} (red, best fit), and 8×10^{-8} (blue). The airmass factor is 1.5.

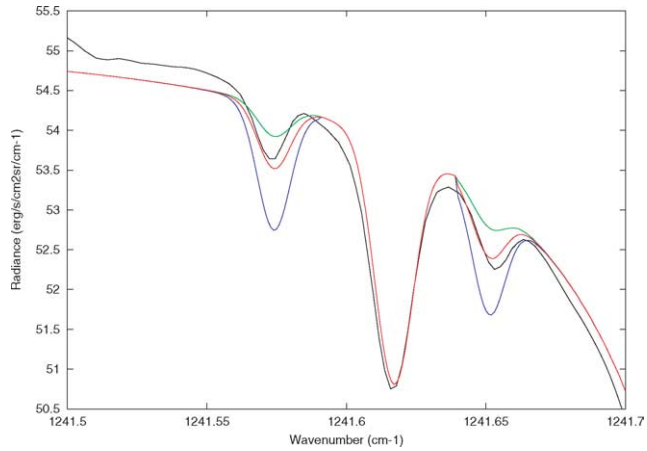

Fig. 3. Same as Fig. 2, except for the range 1241.5–1241.7 cm^{-1}. The strong absorption beyond 1241.7 cm^{-1} is due to a telluric methane line.

3. Modeling and interpretation

The depths of the H_2O_2 lines depend upon the H_2O_2 vertical distribution, the surface temperature T_s, the atmospheric temperature $T(z)$, and in particular, the temperature contrast $T_s - T(z = 0\ \text{km})$. For the selected area of maximum H_2O_2 line intensity (corresponding to an airmass of 1.5), we assumed $T_s = 290$ K and a surface pressure $P_s = 5$ mbar. We then adjusted the values of $T(0\ \text{km}) = 235$ K and $T(20\ \text{km}) = 180$ K to fit the observed depths of the weak CO_2 lines. This thermal structure is close to that predicted by the GCM (Forget et al., 1999) in the selected area, in particular the surface-atmosphere contrast (58 K in the GCM). This temperature profile was then used to model the H_2O_2 lines, following the strategy used in our previous study (Encrenaz et al., 2002). As a first approximation, and for comparison with previous studies, we assumed a constant vertical mixing ratio of H_2O_2. Spectroscopic data of H_2O_2 and CO_2 come from the GEISA data bank (Jacquinet-Husson et al., 1999). In addition, spectroscopic parameters of weak CO_2 isotopic lines, not in the GEISA linelist, were calculated using the analysis by Rothmann (1986). As shown in Figs. 2 and 3, the best fit is obtained with an H_2O_2 mixing ratio of 4×10^{-8}, corresponding to an H_2O_2 column abundance of 7.5×10^{15} cm^{-2}, in the selected area close to the sub-solar point. The error budget on this result is described below.

Since the H_2O_2 and the weak CO_2 lines are optically thin, their column densities are to first order proportional to the line depths. By dividing the depth of a given H_2O_2 line by the depth of a neighboring CO_2 line of comparable intensity, a reliable determination of the H_2O_2 mixing ratio can be obtained as it minimizes the uncertainties in the analysis due to effects of surface and atmospheric properties, including dust opacity and the airmass factor. Using this method to analyze the two sets of H_2O_2 line doublets (see Figs. 2 and 3), we built a map of the H_2O_2 mixing ratio over the martian disk. To determine the H_2O_2 mean line depth, we averaged the four H_2O_2 transitions mentioned above with appropriate

weighting. For the CO_2 line depth, we used the transition at 1241.6 cm^{-1}, which is the weakest one and thus the closest in intensity to the H_2O_2 lines. The resulting map is shown in Fig. 4, along with the map of the continuum and the maps of the H_2O_2 and CO_2 line depths. The H_2O_2 mixing ratio ranges from 2×10^{-8} to 5×10^{-8} over the area where this parameter can be measured. It is maximum at the morning limb at the sub-solar latitude ($\sim 10°$ S) and is lowest poleward of $\sim 45°$ S. The averaged value is about 3.2×10^{-8} and corresponds to a column density of 6×10^{15} cm^{-2} assuming a mean surface pressure of 5 mbar. It is interesting to note that beyond the evening terminator (the right side of the map), the surface temperature drops faster than the atmospheric temperature and the line contrast almost disappears for both CO_2 and H_2O_2 transitions, preventing the H_2O_2 abundance determination. The continuum map shows that the maximum flux (hence the surface temperature) occurs $\sim 20°$ east of the sub-solar point, as expected from global climate models.

There are two possible sources of error in our determination of the H_2O_2 abundance distribution: (1) noise and systematic errors in the data; (2) uncertainties associated with the model parameters. The formal signal-to-noise ratio, in the spectra of Figs. 3–4, exceeds 10,000. However, the precision to which the H_2O_2 line depths can be determined is limited by uncertainties in the continuum level around the lines. This continuum is affected by the nearby telluric lines, imperfect correction of the flat-fielding, and possibly spectral variations of the surface emissivity. We estimate that we can reach a precision of 0.15% on the location of the continuum. As the H_2O_2 line contrast is 1.3 to 1.5%, the uncertainty due to this error source is estimated to $\sim 10\%$. We have estimated the uncertainties associated to the model by varying systematically the various parameters P_s ($\pm 33\%$), T_s (± 10 K) and $T(z)$ (± 10 K). We derive that, for a given value of the H_2O_2 mixing ratio, the H_2O_2/CO_2 line depth varies by 5% at most for the P_s variations, 3% at most for the T_s variations and 4% at most for the variations of $T(z)$. Adding all these errors quadratically, we infer a mean H_2O_2 mixing ratio of $4(\pm 0.5) \times 10^{-8}$, corresponding to an H_2O_2 column abundance of $7.5(\pm 1) \times 10^{15}$ cm^{-2} near the sub-solar point. This value is slightly larger than the mean value of 3.2×10^{-8} quoted above, which reflects the mean value of this mixing ratio above the whole area where this parameter can be measured. The error bars may actually be larger than the numbers given above, due to uncertainties in the H_2O_2 and CO_2 intrinsic line strengths that we cannot estimate. Note that the mean H_2O_2 mixing ratio that we infer by our method is probably not too meaningful. Indeed, most photochemical models predict a non-uniform vertical mixing ratio, with an effective scale height smaller than the mean atmospheric scale height. Nevertheless, the column density derived from our mean mixing ratio can be directly compared to photochemical predictions.

The error bars associated with the H_2O_2 mixing ratios indicated in our map are larger than the one mentioned above for several reasons: (1) the signal-to-noise ratio in a spatial element is 3–4 times lower, (2) in most areas, the CO_2 line depth is smaller than that in the averaged spectra, and (3) near the limb, uncertainties associated with large airmasses have to be taken into account. The 1-SD noise level leads to an error bar on the H_2O_2 mole fraction between ± 0.05 and $\pm 0.25 \times 10^{-8}$, depending on the CO_2 line depth. The 0.15% uncertainty on the continuum yields a larger uncertainty, in the range $0.4–0.8 \times 10^{-8}$. The largest values correspond to the east and south boundaries of the H_2O_2 abundance map (Fig. 4d), and smaller values to longitudes westward of the sub-solar point in the 30° N–40° S latitude range. Finally, the westernmost pixels in this map are affected by the large airmass factor. For a given value of the H_2O_2 mixing ratio, the H_2O_2/CO_2 line depth ratio increases by 15% when the airmass is varied from 1.5 (i.e., that of the averaged spectra) to 4. We can then estimate that the mole fraction for these limb pixels bears an additional uncertainty in the range 0.4×10^{-8} (high latitudes) to 0.7×10^{-8} (sub-solar latitude). As a result, the uncertainty on the H_2O_2 varies from a minimum of $\sim 0.5 \times 10^{-8}$ in the region [30° N–40° S, 0°–30° W of the sub-solar point] to $\sim 0.9 \times 10^{-8}$ at the east and south limits of our H_2O_2 map.

4. Discussion

Our results are in good agreement with predictions of both 1D and 3D photochemical models. Our mean mole fraction ($\sim 3.2 \times 10^{-8}$) also reasonably agrees with the disk-averaged measurement of the H_2O_2 mixing ratio ($1.8 \pm 0.4 \times 10^{-8}$) obtained by Clancy et al. (2004) ten weeks after our measurement. It is difficult, however, to compare precisely the two results, because of the different geometries of the two observations. Our measured H_2O_2 mixing ratio ranges from 2×10^{-8} to 5×10^{-8} in the area where this parameter can be inferred, with a maximum around the sub-solar point. Clancy et al.'s measurement corresponds to a field of view of 13.3 arcsec (about half of the planet's diameter) centered on the martian disk and thus does not include the sub-solar point. This may explain at least partly why the submillimeter measurement is slightly lower than ours.

The martian Global Climate Model (GCM, Forget et al., 1999) includes a photochemical module which computes the full spatial and temporal variations of the atmospheric composition, based on a water cycle also computed within the GCM, and in agreement with the one observed by the TES instrument aboard the MGS mission (Smith, 2002). No heterogeneous chemical processes are considered in this model. The spatial distribution of the H_2O_2 mixing ratio inferred from this calculation is shown in Fig. 5. Both observed and computed H_2O_2 mixing ratios behave similarly in the southern hemisphere, with a maximum in the morning limb and around 20° S latitude. However, in the northern hemisphere, the model predicts a maximum of the H_2O_2 mixing ratio which does not appear in the observations; this discrepancy

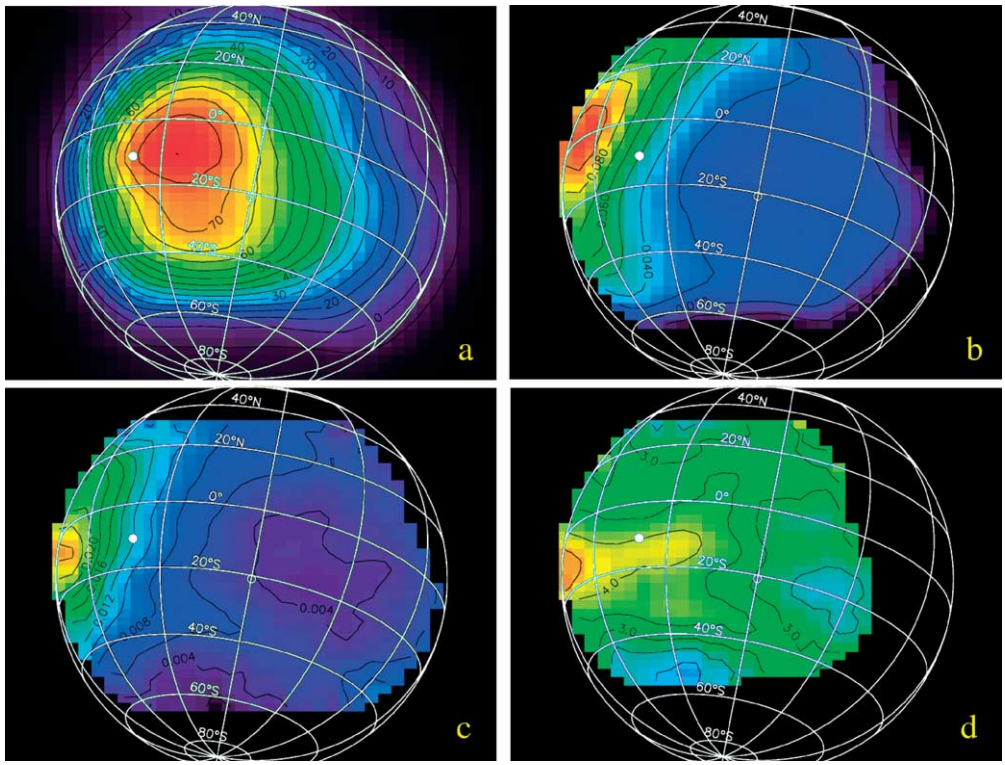

Fig. 4. Maps of (a) the continuum, (b) the CO_2 line depth, (c) the H_2O_2 line depth, and (d) the H_2O_2/CO_2 mixing ratio over the martian disk, summed over the June 19 and 20 observations. The sub-solar point is indicated by a white dot and the sub-Earth point as a circle. In panel (a), the continuum is in erg s^{-1} cm^{-2} sr^{-1}/ cm^{-1}; contours are separated by 5 of these units. The CO_2 line depth, expressed as a fraction of the continuum (b), is obtained from the CO_2 line at 1241.6 cm^{-1}. The H_2O_2 line depth (c) is obtained from the average of the four H_2O_2 lines shown in Figs. 2–3. In (d), the H_2O_2 mixing ratio is indicated in multiples of 10^{-8}; contours are separated by 0.5×10^{-8}. In maps (c)–(d), the data have been smoothed to 1.5-arcsec resolution and are limited to the regions where the S/N is statistically significant.

remains to be understood. The enhancement of H_2O_2 in the morning sector could possibly be explained by the lack of H_2O_2 photolysis loss throughout the night (Atreya and Gu, 1995), which could result in its build up towards morning. It can also be noted that the region of maximum H_2O_2 mixing ratio is an area of low altitude (south of Amazonis Planitia), and topographic effects may also be involved. To distinguish between the two possibilities, observations at a different sub-Earth longitude are needed.

Our observed mean abundance of H_2O_2 ($\sim 6 \times 10^{15}$ cm^{-2}) is six times larger than the low upper limit we inferred in February 2001. We attribute this difference to seasonal variations in H_2O_2 as the two measurements correspond to very different times of the seasonal cycle. Preliminary calculations indicate that several factors play a role in determining the abundance of H_2O_2 and its seasonal variation, so that ultimately the correlation between H_2O and the H_2O_2 column abundances may not be strong. The most important factors are, (i) atmospheric temperature, (ii) height dependent lifetimes of key species, and (iii) height dependent loss processes, including photolysis rates of individual species. For example, a factor of 1000 change in the abundance of H_2O at the *surface* (from 0.1 to 100 pr. μm) results in only a very small change in the water vapor in the *photochemical regime*. This is because the water vapor

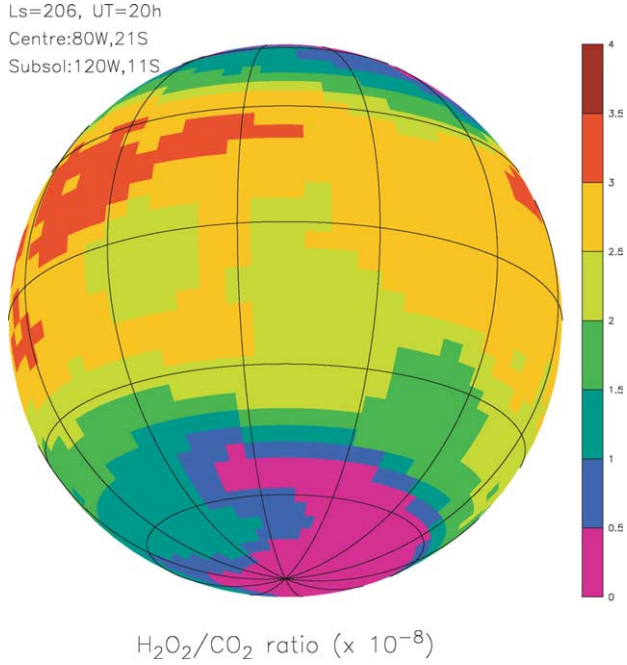

Fig. 5. Map of the H_2O_2 mixing ratio, as modeled by the GCM under the conditions of our observations. This map can be compared to Fig. 4d. The longitude of the central meridian is 80° W and that of the sub-solar point is 120° W.

available in this region is saturation limited, due to its condensation below 20–30 km irrespective of the H_2O column abundance at the surface. Clancy et al. (2004) also remarked that the non-detection of H_2O_2 in 2001 could partly be due to the fact that the 2001 observations were done close to aphelion ($Ls = 112°$) in the northern martian hemisphere where the temperature is very low. The lower atmospheric temperatures of the 2001 epoch would have resulted in the condensation of water vapor at ~ 10 km (Encrenaz et al., 2001), a much lower altitude than in the case of the current 2003 observations, thus favoring a larger photochemical production of H_2O_2 in 2003.

Similarly, a factor of 1000 increase in the H_2O column at the surface, results in only a doubling of the H density at the surface, even though H_2O photolysis is the source of H. This is mainly due to the fact that the photochemical lifetime of H near the surface is extremely short, on the order of 1 s, so that the species reacts quickly with ambient molecules and gets depleted. The fate of all odd hydrogen species is important for the ultimate amount of H_2O_2. Finally, the loss of H_2O_2, which is by photolysis, proceeds at a different rate than that of H_2O. The steady state density of atmospheric species, including H_2O_2, results from a combination of both the production rate and the loss rate. The end result is that the H_2O_2 column abundance shows only a weak correlation to the H_2O column abundance at the surface. Based on the model of Atreya and Gu (1994,1995), it is found that at midlatitudes, the H_2O_2 column abundance increases by approximately a factor of ten from winter to summer during which time the water vapor amount increased by a factor of over 100. These models also indicate that the seasonal changes are much more dramatic at higher latitudes, because of smaller solar UV flux and lower temperatures. For example, at 65° N, the winter to summer increase in the H_2O_2 column abundance is a factor of 10^5.

In the future, mapping the H_2O_2 abundance at seasons different from the present observations is clearly an important objective. This is required to better constrain photochemical-dynamical models and understand the role of this important molecule in the atmospheric chemistry and in the oxidization of the martian soil.

Acknowledgments

Observations with TEXES were supported by NSF Grant AST-0205518. T.E. and B.B. acknowledge support from the Centre National de la Recherche Scientifique.

References

Atreya, S.K., Gu, Z., 1994. Stability of the martian atmosphere: is heterogeneous catalysis essential? J. Geophys. Res. 99, 13133–13145.

Atreya, S.K., Gu, Z., 1995. Photochemistry and stability of the atmosphere of Mars. Adv. Space Res. 16 (6), 57–68.

Bullock, M.A., Stoker, C.R., McKay, C.P., Zent, A.P., 1994. A coupled soil-atmosphere of H_2O_2 on Mars. Icarus 107, 142–154.

Clancy, R.T., Nair, H., 1996. Annual (perihelion–aphelion) cycles in the photochemical behavior of the global Mars atmosphere. J. Geophys. Res. 101, 12785–12790.

Clancy, R.T., Sandor, B.J., Moriarty-Schieven, G.H., 2004. A measurement of the 362 GHz absorption line of Mars atmospheric H_2O_2. Icarus 168, 116–121.

Encrenaz, T., Lellouch, E., Paubert, G., Gulkis, S., 2001. The water vapor vertical distribution on Mars from millimeter transitions of HDO and $H_2{}^{18}O$. Planet. Space Sci. 49, 731–741.

Encrenaz, T., Greathouse, T.K., Bézard, B., Atreya, S.K., Wong, A.S., Richter, M.J., Lacy, J.H., 2002. A stringent upper limit of the H_2O_2 abundance in the martian atmosphere. Astron. Astrophys. 396, 1037–1044.

Encrenaz, T., Bézard, B., Greathouse, T.K., Lacy, J.H., Richter, M.J., Atreya, S.K., Wong, A.S., 2003. Mars. IAU Circ. 8254.

Forget, F., Hourdin, F., Fournier, R., Hourdin, C., Talagrand, O., Collins, M., Lewis, S.R., Read, P., Huot, J.-P., 1999. Improved general circulation models of the martian atmosphere from the surface to above 80 km. J. Geophys. Res. 104, 24155–24176.

Huguenin, R.L., 1982. Chemical weathering and the Viking biology experiments on Mars. J. Geophys. Res. 87, 10069–10082.

Jacquinet-Husson, N., 47 colleagues, 1999. The 1997 spectroscopic GEISA databank. J. Quant. Spectrosc. Radiat. Transfer 62, 205–254.

Jakosky, B.M., Haberle, R.M., 1992. The seasonal behavior of water vapour in Mars. In: Kieffer, H.H., Jakosky, B.M., Snyder, C.W., Matthews, M.S. (Eds.), Mars. Univ. of Arizona Press, Tucson, pp. 969–1016.

Krasnopolsky, V.A., 1993. Photochemistry of the martian atmosphere (mean conditions). Icarus 101, 313–332.

Krasnopolsky, V.A., 1995. Uniqueness of a solution of a steady state photochemical problem: applications to Mars. J. Geophys. Res. 100, 3263–3276.

Krasnopolsky, V.A., Bjoraker, G.L., Mumma, M.J., Jennings, D.E., 1997. High-resolution spectroscopy of Mars at 3.7 and 8 μm: a sensitive search of H_2O_2, H_2CO, HCl, and CH_4, and detection of HDO. J. Geophys. Res. 102, 6525–6534.

Lacy, J.H., Richter, M.J., Greathouse, T.K., Jaffe, D.T., Zhu, Q., 2002. TEXES: a sensitive high-resolution grating spectrograph for the mid-infrared. Publ. Astron. Soc. Pacific 114, 153–168.

Levin, G.V., Straat, P.A., 1988. A reappraisal of life on Mars. In: Reiber, D.B. (Ed.), The NASA Mars Conference. Univ. of San Diego, San Diego, CA, pp. 186–210.

Nair, H., Allen, M., Anbar, A.D., Yung, Y.L., Clancy, R.T., 1994. A photochemical model of the martian atmosphere. Icarus 111, 124–150.

Oyama, V.I., Berdahl, B.J., Carle, G.C., 1977. Preliminary findings of the Viking gas exchange experiment and a model for martian surface chemistry. Nature 265, 100–114.

Rohlfs, K., Wilson, T., 2004. Tools of Radioastronomy. Springer-Verlag, Berlin.

Rothmann, L.S., 1986. Infrared energy levels and intensities of carbon dioxide. Part 3. Appl. Optics 25, 1795–1816.

Smith, M.D., 2002. The annual cycle of water vapor on Mars as observed by the Thermal Emission Spectrometer. J. Geophys. Res. 107, 25.1–25.19.